Molecular Crystals and Liquid Crystals

Publication details, including instructions for authors and subscription information:
http://www.tandfonline.com/loi/gmcl20

Interferometric Method for the Measurement of the Flexoelectric Polarisation Using Nematic Liquid Crystal Phase Gratings

C. L. Trabi [a], A. A. T. Smith [b] & C. V. Brown [a]

[a] School of Science and Technology, Nottingham Trent University, Erasmus Darwin Building, Clifton Lane, Clifton, Nottingham, United Kingdom

[b] Department of Mathematics, University of Strathclyde, Livingstone Tower, Glasgow, United Kingdom

Version of record first published: 05 Oct 2009

To cite this article: C. L. Trabi, A. A. T. Smith & C. V. Brown (2009): Interferometric Method for the Measurement of the Flexoelectric Polarisation Using Nematic Liquid Crystal Phase Gratings, Molecular Crystals and Liquid Crystals, 509:1, 378/[1120]-392/[1134]

To link to this article: http://dx.doi.org/10.1080/15421400903066125

Mol. Cryst. Liq. Cryst., Vol. 509, pp. 378/[1120]–392/[1134], 2009

ISSN: 1542-1406 print/1563-5287 online
DOI: 10.1080/15421400903066125

Interferometric Method for the Measurement of the Flexoelectric Polarisation Using Nematic Liquid Crystal Phase Gratings

C. L. Trabi[1], A. A. T. Smith[2], and C. V. Brown[1]
[1]School of Science and Technology, Nottingham Trent University, Erasmus Darwin Building, Clifton Lane, Clifton, Nottingham, United Kingdom
[2]Department of Mathematics, University of Strathclyde, Livingstone Tower, Glasgow, United Kingdom

An interferometric method using a nematic liquid crystal phase grating has recently been developed for determining the sum of the flexoelectric coefficients, (e_1+e_3) [C. Trabi, C. V. Brown, A. A. T. Smith and N. J. Mottram, Appl. Phys. Lett. **92***, 223509 (2008)]. The switching response of the device can be simulated if the applied 0.2 Hz squarewave voltage in the nematic layer is modified so that it is enhanced by a reverse ion-field after each polarity reversal and then decays with time. This process has been investigated using measurements of the transient capacitance of a planar nematic layer to the same waveform.*

Keywords: dielectrics; diffraction optical element; nematic liquid crystals; transient capacitance

1. INTRODUCTION

Nematic liquid crystal materials exhibit orientational ordering and anisotropic physical properties [1,2]. Calamitic nematics tend to order with the long axes of their molecules, on average, aligned along a direction referred to as the n-director. For a nematic material composed from molecules that posses longitudinal permanent dipoles

The authors gratefully acknowledge Merck Chemicals Ltd. (Chilworth, U.K.) for supplying test cells and the HEFCE for funding (EPSRC RAE funds allocated by Nottingham Trent University and EPSRC grant GR/R17423/01).

Address correspondence to C. V. Brown, School of Science and Technology, Nottingham Trent University, Erasmus Darwin Building, Clifton Lane, Clifton, Nottingham, NG11 8NS, UK. E-mail: carl.brown@ntu.ac.uk

a Langevin-type contribution to the low frequency induced polarisation can lead to a larger value of the permittivity measured parallel to the n-director ($\varepsilon_{||}$) compared to the value measured perpendicular to the n-director ($\varepsilon_{\perp}$) [3]. In the undistorted medium the molecules are as likely to align parallel to the n-director as they are to align anti-parallel, and so there is no net bulk polarisation. If, in addition, the molecules possess a shape asymmetry then a spatial distortion of the n-director can lead to the appearance of a flexoelectric polarisation, $\mathbf{P}_f = e_1(\nabla \cdot \mathbf{n})\mathbf{n} + e_3(\nabla \times \mathbf{n}) \times \mathbf{n}$, where the flexoelectric coefficients e_1 and e_3 relate to splay and bend distortions respectively [2,4].

A phase grating geometry was used by Prost and Pershan to perform the first measurements of the sum of the coefficients $(e_1 + e_3)$ [5]. Optical diffraction techniques were used to distinguish between the spatial period of the flexoelectric distortion which was twice the spatial period of the dielectric distortion when the nematic layer was subject to a periodic in-plane voltage profile. The value of the sum $(e_1 + e_3)$ can also be found from measurements in the hybrid aligned geometry (HAN) [6–10]. The in-built distortion through the nematic layer in this geometry gives rise to a flexoelectric polarisation which can be detected through the optical or capacitance response to different polarities of an electric field applied across the layer. The interpretation of measurements in the HAN geometry is complicated by the presence of any ionic contamination in the nematic material [10–13].

In previous measurements, reported by the current authors [14], a Mach-Zehnder interferometer was used to measure the time dependent periodic distortion profile in a nematic liquid crystal phase grating. In reference [5] optical diffraction techniques were used and the nematic liquid crystal layer was homeotropically aligned. In reference [14] the nematic liquid crystal was planar aligned and the average refractive index profile across the grating device at each point in time was determined directly from the displacement of tilt fringes in the interferometer. A 0.2 Hz squarewave voltage was applied to alternate stripe electrodes in an interdigitated electrode geometry and the different switching response of the layer to the positive and negative polarities of the applied waveform allowed the value of the sum of the flexoelectric coefficients $(e_1 + e_3)$ to be determined. To fit the switching response data the effective voltage that was experienced by the nematic layer was modified. In order to account for ionic shielding and migration it was assumed that the applied voltage was enhanced by a reverse ion-field after each polarity reversal and then decayed exponentially with time during each half period due to ionic migration.

In the current work the effects of ionic migration and shielding are investigated using transient capacitance techniques in which a high frequency low amplitude signal is used to probe the time dependent capacitance of a planar aligned nematic layer during addressing with a 0.2 Hz squarewave voltage across the layer. Modelling of these experimental conditions using nematic continuum theory with a single viscosity and the non-equilibrium charge transport equations provides justification for the modified form used for effective voltage described above. The interferometric measurement approach is then applied to a planar nematic layer confined between substrates coated with an aligning polymer that was unidirectionally rubbed parallel on opposing substrates. The results of this measurement geometry are then compared directly with results from the antiparallel alignment case described in reference [14].

2. TRANSIENT CAPACITANCE MEASUREMENTS

The material E7 (Merck) was used for the investigation. Measurements were performed on a test cell with planar surface alignment that was fabricated from two glass substrates of thickness 1.1 mm. The gap between the substrates, which contained the liquid crystal, was 22 μm. On the inner sides of each substrate were the transparent indium tin oxide electrodes and an alignment layer that was in contact with the liquid crystal material. The electrodes were circular and a guard ring was used on one of the substrates to reduce inaccuracies in the capacitance measurements due to fringing fields. The planar surface alignment was generated with a thin polymer layer that was rubbed in parallel directions on the opposite substrates.

The use of the differentiator circuit to find the time-dependent capacitance of a liquid crystal test cell in response to an amplitude modulated waveform was described in reference [15]. This procedure can also be used for arbitrary voltage switching waveforms. The switching waveform in the current work is a 0.2 Hz squarewave. This is summed with a probe waveform, $V_I = V_P \cos \omega t$, which has much higher frequency (10 kHz) and a low amplitude ($V_p = 0.2$ Vrms). The resultant waveform is applied to one plate of the liquid crystal capacitor. The other plate is connected to the input of a differentiator op-amp circuit [16]. Since the input to the differentiator is at virtual earth the full voltage of the switching waveform appears across the liquid crystal layer. The differentiator output voltage that is in quadrature with the input voltage, $V_O = -V_{OQ} \sin \omega t$, has a magnitude that is proportional to the permittivity ε of the nematic layer. The time dependent value of the permittivity is obtained using the expression

$\varepsilon = |V_{OQ}|/(RC_O\omega|V_P|)$ where R is the value of the resistor in the differentiator circuit and C_O is the capacitance of the liquid crystal test cell when empty. This expression is valid provided that any ionic species in the liquid crystal material cannot polarise quickly enough to respond to the probe waveform. It has been confirmed from measurements of the loss of the layer as a function of frequency that the ionic species in the material E7 used in the study do not respond significantly to the probe frequency of 10 kHz.

The input waveforms were generated using a four-channel arbitrary waveform generator (model TGA1244, TTi). The output waveforms were captured using a 12 bit digital storage oscilloscope (model 54622A, Agilent) and phase sensitive detection was performed using a DSP lock-in amplifier (model 7265, signal recovery). The differentiator circuit comprised of a FET operational amplifier having high input impedance (model OPA445AP, Burr-Brown, Texas Instruments) and a high stability wire-wound resistor with value R = 800 Ω. Figure 1 shows the capacitance as a function of time for applied squarewave driving voltages in the range 1.02 to 1.86 V. The period of the squarewave was 0.2 Hz and the changes in polarity occurred at 0.0 sec, 2.5 sec and 5.0 sec in Figure 1. The data was recorded at a temperature of 20°C.

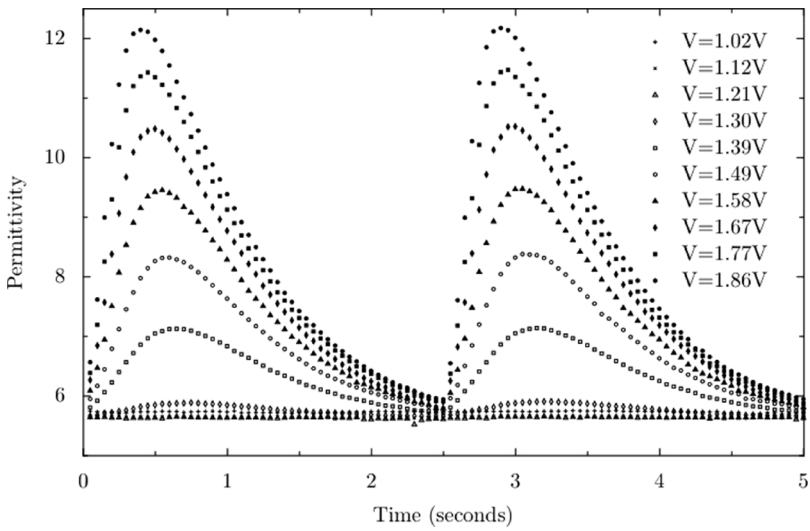

FIGURE 1 Transient capacitance response of a 22 μm planar layer of the nematic liquid crystal E7 to an applied squarewave voltage waveform with frequency 0.2 Hz and amplitudes between 1.02 V (cross) and 1.86 V (filled circle).

The Freedericksz threshold voltage [17] has been previously measured as 0.93 V in the same cell geometry and on the same batch of the material E7 with a 1 kHz a.c. applied voltage at 24°C [15]. In the absence of ionic contamination this value would also give the threshold for the amplitude of a squarewave voltage above which reorientation of the nematic director in the bulk of the layer would occur. If the squarewave voltage having an amplitude above the threshold is applied for a sufficient time the permittivity of the layer should rise to a constant value corresponding to the value that would be obtained from static measurements using capacitance bridge [17,18].

In Figure 1 there is little change in the permittivity up to 1.21 V and above this voltage there is a peak in the permittivity within each half period of the 0.2 Hz squarewave voltage. This switching behaviour can be explained by the presence of ionic contamination in the liquid crystal material. During the application of a d.c. voltage in each half period the ionic species migrate by drift under the action of the electric field towards the electrodes. As the ions accumulate in the region of the electrodes they shield the external voltage, since a positive ion will drift to a negative electrode and vice versa. This "ionic-field" reduces the voltage that is experienced by the liquid crystal layer [19]. When the polarity of the applied voltage is instantaneously reversed the ions are initially adjacent to electrodes that have the same polarity, i.e., a positive ion is now adjacent to a positive electrode. There is a reverse ionic field which adds to the field from the electrodes which causes an initial reorientation of the nematic n-director during each half period. The increasing tilt angle leads to the increase in the permittivity. A peak in the permittivity occurs because this is followed by the reduction in the director tilt angle again as the ions move to shield the applied voltage.

3. TRANSIENT CAPACITANCE SIMULATIONS

The transient capacitance of a nematic layer containing mobile ionic species was investigated using dynamic nematic continuum theory with a single viscosity, γ_1 [20,21]. The continuum theory equation, the non-equilibrium charge transport equations, and the appropriate Maxwell equations in 1 dimension were solved self-consistently using commercial PDE solver software [22,23]. The time evolution of the n-director profile through the liquid crystal layer, $\theta(z, t)$, was calculated in response to a squarewave voltage waveform applied to the electrodes at $z = 0$ and $z = d$. The potential profile through the layer,

$V(z, t)$, and the densities of positive ions, $n_p(z, t)$, and negative ions, $n_n(z, t)$, were solved simultaneously. The simulation does not model the surface trapping of ions [24,25] and the surfaces were treated as being electrically blocking. The permittivity as a function of the position within the layer, $\varepsilon[\theta(z, t)]$, was calculated using the values $\varepsilon_{||} = 19.1$ and $\varepsilon_{\perp} = 5.2$. The permittivity of the nematic layer was then calculated by dividing the layer into slices and treating it as an array of capacitors in series. The values of the physical parameters were as follows [15]: splay elastic constant $K_1 = 10.5$ pN; bend elastic constant $K_3 = 15.2$ pN; and viscosity $\gamma_1 = 0.18\,\mathrm{N\ s\ m^{-2}}$.

Figure 2 shows a theoretical prediction of the transient capacitance in response to a squarewave voltage with frequency 0.2 Hz and amplitude 1.5 V. The equilibrium ion densities of positively and negatively charged mobile ionic species were set to be equal, $n_{\mathrm{nO}} = n_{\mathrm{pO}} = n_O$ with values between $n_{\mathrm{O}} = 1.0 \times 10^{21}\,\mathrm{m^{-3}}$ and $n_{\mathrm{O}} = 1.0 \times 10^{23}\,\mathrm{m^{-3}}$, as shown in the legend for Figure 2. The value of the mobility was chosen to obtain curves with peak values in similar positions to the experimental curves shown in Figure 1. For both the charged species the mobility μ was set as $\mu = \mu_n = \mu_p = 1 \times 10^{-9}\,\mathrm{m^2\ V^{-1}\ s^{-1}}$ and the value of the diffusion constant was fixed via the Einstein

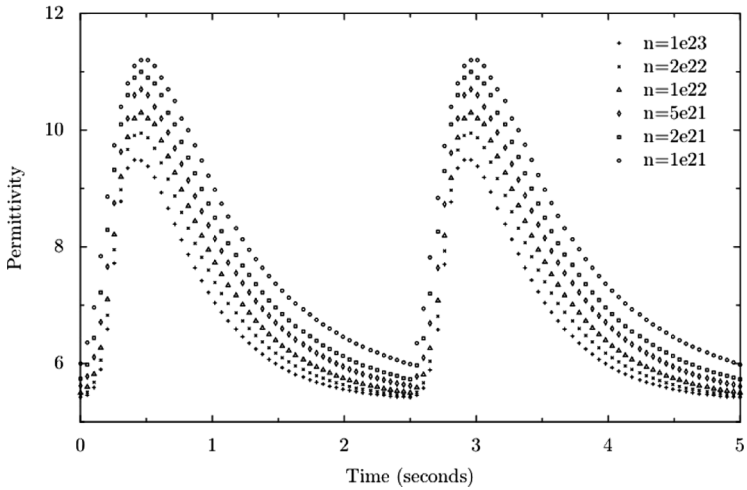

FIGURE 2 Theoretical prediction of the transient capacitance in response to a squarewave voltage waveform with frequency 0.2 Hz and amplitude 1.5 V. The values of the equilibrium densities that were used for both the positively and negatively charged mobile ionic species are shown in the legend.

relation, $D = (k_B T/|q|)\mu = 0.026\mu$ for singly charged species at room temperature.

Figure 3 shows the value of the gradient of the potential in the centre of the cell multiplied by the cell thickness, $d \times \nabla V(z = d/2, t)$. This gives an indication of the potential that is experienced by the bulk region of the nematic liquid crystal layer after the shielding effects of the mobile ionic charge. It is an indication, rather than a quantitative measure, because the charge distribution is only localised close to the electrodes at the boundaries towards the end of a half period of the applied waveform. In addition, the potential profile through the layer, $V(z, t)$, is a solution of the Maxwell equation $\nabla \cdot \mathbf{D} = |e|(n_p - n_n)$ and this is highly distorted away from being a linear profile due to the dielectric anisotropy of the liquid crystal and the presence of the ionic species. However, given these caveats, the numerical work indicates that a voltage waveform similar to that shown in Figure 3 can be used as an appropriate simplified model to simulate the effects of charge migration and shielding without solving the full non-equilibrium charge transport equations. This approach will be used in the 2 dimensional simulations in section 5.

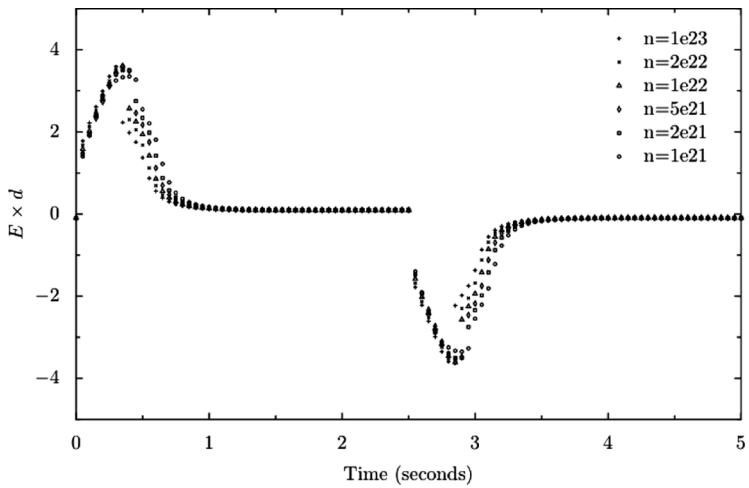

FIGURE 3 Theoretical predictions for the electric field in the centre of the cell multiplied by the cell thickness corresponding to the transient capacitance curves shown in Figure 2. The values of the equilibrium densities that were used for both the positively and negatively charged mobile ionic species are shown in the legend.

4. INTERFEROMETRIC MEASUREMENTS

The geometry of the device used for the interferometric measurements is shown in Figure 4. The thickness of the layer of the nematic liquid crystal E7, at 17.8 μm, was slightly thinner than the device used in section 2. The glass substrates were again coated with indium tin oxide electrodes and with a polymer alignment layer that was rubbed in parallel directions on the opposing substrates. The resulting surface pre-tilt directions are indicated in Figure 4. In previous work the anti-parallel alignment geometry was used [14]. The electrode geometry differed from the device in section 2: the upper substrate is continuous and was an earth plane, and the electrode on the lower plate was etched to form an interdigitated array of parallel stripes. Alternate electrodes in the array were held at earth potential and at voltage V_O. The electrode width was 37 μm and the gaps between the electrodes were 43 μm wide.

The periodic reorientation pattern of the liquid crystal in the device in response to a periodic applied voltage gives rise to a periodic refractive index profile for light polarised along the x-direction. The resultant periodic change in the optical path length has been measured directly by placing the device in one arm of a Mach-Zehnder interferometer [26] and tilting one of the mirrors of the interferometer. This gives an array of sinusoidal fringes across the device and the y-displacement of the fringes at a position x can be directly related to the optical path length through a z-section of the device at that x-position.

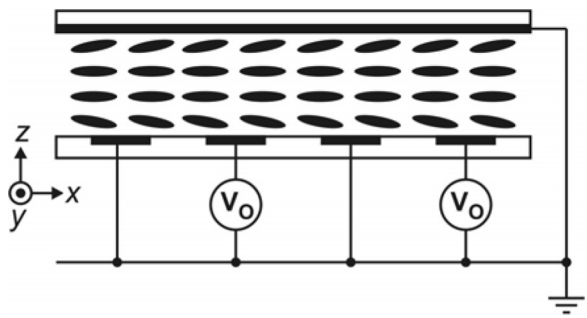

FIGURE 4 Schematic diagram of the device geometry. The filled black rectangles show the positions of indium tin oxide electrodes. The striped electrodes on the lower substrate were fabricated in an interdigitated geometry so that alternate electrodes could be differently biased.

The interferometer was illuminated with a He-Ne laser light with wavelength $\lambda_O = 632.8\,\text{nm}$ and polarised in the x-direction. With no voltages applied to the device the normally incident light travelling through the nematic layer experiences the refractive index parallel to the director, $n_{||}$, and so the optical path length through the nematic layer is $k(V=0)\cdot d = k_{||}\cdot d = 2\pi n_{||} d/\lambda_O$. When a voltage is applied a tilt distortion of the nematic n-director is produced in the layer, $\theta(x, z, t)$. For normally incident light the nematic layer will again be treated as an array of slices where the refractive index in the x-direction in each slice is given by: $1/n_{eff}^2 = (\cos^2\theta/n_{||}^2) + (\sin^2\theta/n_{\perp}^2)$. The optical path length for x-polarised light travelling through the layer is given by the sum of the optical path lengths for all of the slices and this can be expressed by an average effective wavevector for the layer, $\bar{k}_{eff}(V = V_O)$, or an average refractive index for the layer, $\bar{n}_{eff}$. A tilt fringe in the interferometer is displaced in position by one fringe spacing when the difference between the voltage-on and voltage-off optical path lengths through the nematic liquid crystal layer equals 2π radians, so that $\bar{n}_{eff} - n_{||} = \lambda_O/d$.

The fringe displacement profiles are shown in Figure 5. Each of the fringes shown is the average of 5 of the parallel tilt fringes that crossed the field of view of the device in the x-direction when it was observed in the interferometer. The time at which fringe was recorded corresponds to the time value at which it intersects with the x-axis.

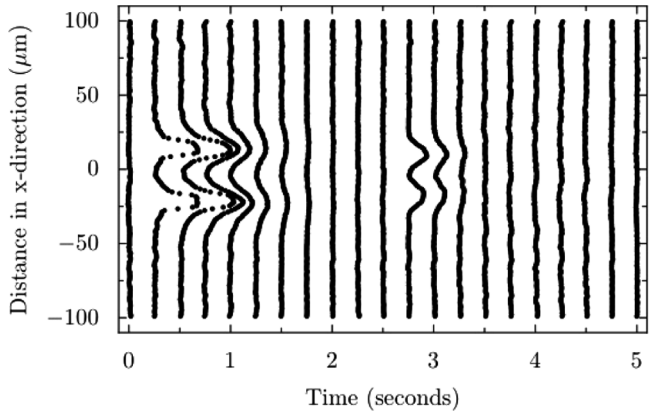

FIGURE 5 The displacement profiles of parallel tilt fringes that crossed the field of view of the device in the x-direction when it was observed in the interferometer. The time at which each fringe was recorded corresponds to the time value at which it intersects with the x-axis. For clarity the amplitude of each fringe has been multiplied by a factor of two.

The measurement was recorded whilst a square wave voltage waveform with frequency 0.2 Hz and amplitude 1.17 V was applied to the electrodes marked as V_O in Figure 4. In Figure 5 the applied voltage was positive in the time period 0 to 2.5 sec and negative in the time period 2.5 to 5.0 sec.

In Figure 5, peaks in the fringe displacement can be observed at $+17\,\mu m$ and $-17\,\mu m$. The peak amplitudes increase quickly after each change in the polarity of the squarewave voltage waveform and then decay over a slightly longer time scale during each half period. These dependences of the peak amplitude on time in the phase grating geometry of Figure 4 are similar to the form of the transient capacitance shown earlier in Figure 1. As discussed in section 3 above, these observations can be attributed to the migration and shielding effects of mobile ionic charges in the nematic material E7. There is a slight asymmetry between the peaks at $+17\,\mu m$ and $-17\,\mu m$, with the peak at $+17\,\mu m$ being slightly larger than the peak at $-17\,\mu m$ during the time period 0 to 2.5 sec (positive voltage) but the asymmetry is the other way around during the time period 2.5 to 5.0 sec (positive voltage).

The main difference between the results shown in Figure 5 and the transient capacitance results, shown in Figure 1, is that in Figure 5 the amplitudes of the peaks in the fringe displacements are much higher for the positive half period of V_O than for the negative half period of V_O. This observation can be explained by the presence of a flexoelectric polarisation in the nematic material. The phase grating device of Figure 4 has an inherent asymmetry, since there are striped interdigitated electrodes on one substrate but a continuous electrode on the other plate, and so the interaction of the flexoelectric polarisation with the fringing electric fields and the distortions in the nematic n-director can be observed directly in this geometry.

5. FITTING THE INTERFEROMETRIC MEASUREMENT DATA

The nematic n-director profile in the phase grating device of Figure 4, $\theta(x, z, t)$, has been calculated using dynamic nematic continuum theory with a single viscosity γ_1 in 2 dimensions [20,21]. For the geometry shown in Figure 4 the n-director is given by the vector expression $\mathbf{n} = (\cos\theta, 0, \sin\theta)$ and the electric field can be calculated from the potential $V(x, z, t)$ via the relation: $\mathbf{E} = (-\partial V/\partial x, 0, -\partial V/\partial z)$. The free energy is given by the sum of elastic, dielectric and flexoelectric energy terms. Minimisation of the free energy with respect to the angle θ using the Euler-Lagrange equation yields Eq. (1).

$$\gamma_1\frac{\partial\theta}{\partial t}=\frac{\partial}{\partial x}\left\{K_1\left(\sin\theta\frac{\partial\theta}{\partial x}-\cos\theta\frac{\partial\theta}{\partial z}\right)\sin\theta+K_3\left(\cos\theta\frac{\partial\theta}{\partial x}+\sin\theta\frac{\partial\theta}{\partial z}\right)\cos\theta\right\}$$
$$+\frac{\partial}{\partial x}\left\{-(e_1+e_3)\sin\theta\cos\theta\frac{\partial V}{\partial x}+\left(e_3\cos^2\theta-e_1\sin^2\theta\right)\frac{\partial V}{\partial z}\right\}$$
$$+\frac{\partial}{\partial z}\left\{-K_1\left(\sin\theta\frac{\partial\theta}{\partial x}-\cos\theta\frac{\partial\theta}{\partial z}\right)\cos\theta+K_3\left(\cos\theta\frac{\partial\theta}{\partial x}+\sin\theta\frac{\partial\theta}{\partial z}\right)\sin\theta\right\}$$
$$+\frac{\partial}{\partial z}\left\{\left(e_1\cos^2\theta-e_3\sin^2\theta\right)\frac{\partial V}{\partial x}+(e_1+e_3)\sin\theta\cos\theta\frac{\partial V}{\partial z}\right\}$$
$$-\frac{1}{2}(K_1-K_3)\sin(2\theta)\left[\left(\frac{\partial\theta}{\partial x}\right)^2-\left(\frac{\partial\theta}{\partial z}\right)^2\right]+(K_1-K_3)\cos(2\theta)\frac{\partial\theta}{\partial x}\frac{\partial\theta}{\partial z}$$
$$+\frac{1}{2}\varepsilon_O\left(\varepsilon_{\|}-\varepsilon_{\perp}\right)\sin(2\theta)\left[\left(\frac{\partial V}{\partial z}\right)^2-\left(\frac{\partial V}{\partial x}\right)^2\right]+\varepsilon_O\left(\varepsilon_{\|}-\varepsilon_{\perp}\right)\cos(2\theta)\frac{\partial V}{\partial x}\frac{\partial V}{\partial z}$$
$$+(e_1+e_3)\sin(2\theta)\left[\frac{\partial\theta}{\partial x}\frac{\partial V}{\partial z}+\frac{\partial\theta}{\partial z}\frac{\partial V}{\partial x}\right]+(e_1+e_3)\cos(2\theta)\left[\frac{\partial\theta}{\partial x}\frac{\partial V}{\partial x}-\frac{\partial\theta}{\partial z}\frac{\partial V}{\partial z}\right] \tag{1}$$

Minimisation of the free energy with respect to the potential V using the Euler-Lagrange equation yields Eq. (2).

$$0=-\frac{1}{2}\varepsilon_O\frac{\partial}{\partial x}\left\{2\left(\varepsilon_{\|}\cos^2\theta+\varepsilon_{\perp}\sin^2\theta\right)\frac{\partial V}{\partial x}+2\left(\varepsilon_{\|}-\varepsilon_{\perp}\right)\sin\theta\cos\theta\frac{\partial V}{\partial z}\right\}$$
$$+\frac{\partial}{\partial x}\left\{\left(e_1\cos^2\theta-e_3\sin^2\theta\right)\frac{\partial\theta}{\partial z}-(e_1+e_3)\sin\theta\cos\theta\frac{\partial\theta}{\partial x}\right\}$$
$$-\frac{1}{2}\varepsilon_O\frac{\partial}{\partial y}\left\{2\left(\varepsilon_{\|}\sin^2\theta+\varepsilon_{\perp}\cos^2\theta\right)\frac{\partial V}{\partial z}+2\left(\varepsilon_{\|}-\varepsilon_{\perp}\right)\sin\theta\cos\theta\frac{\partial V}{\partial x}\right\}$$
$$+\frac{\partial}{\partial y}\left\{\left(e_3\cos^2\theta-e_1\sin^2\theta\right)\frac{\partial\theta}{\partial x}+(e_1+e_3)\sin\theta\cos\theta\frac{\partial\theta}{\partial z}\right\} \tag{2}$$

Equations (1) and (2) were solved self-consistently using commercial PDE solver software [22,23]. The time evolution of the 2 dimensional n-director profile through the liquid crystal layer, $\theta(x, z, t)$, was calculated in response to a squarewave voltage waveform applied to the electrodes at $z=0$ and $z=d$. The use of finite elements to solve the nematic continuum equations can lead to loss of the nematic n-director symmetry, $\mathbf{n}\equiv-\mathbf{n}$, as a result of the discretisation of the equation onto the finite element grid [27–29]. This difficulty does not arise in the current work because the fringing field geometry removes any ambigiuty between the θ orientations in neighbouring

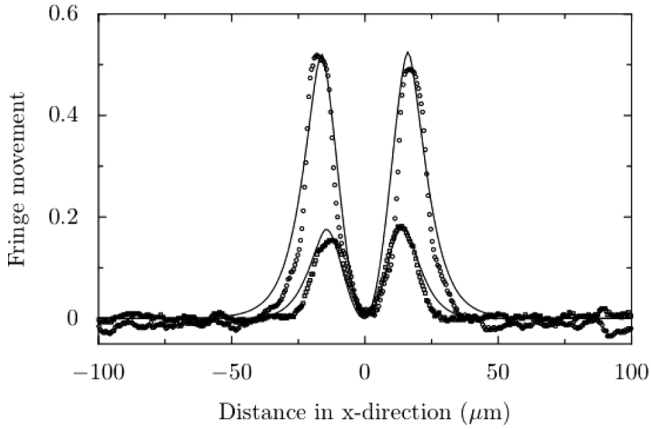

FIGURE 6 The relative fringe movement as a function of distance in the x-direction across the phase grating device from Figure 4, corresponding to vertical sections through Figure 5 at time 0.25 sec (+1.17 V, circles) and time 2.75 (−1.17 V, squares). The solid lines are theoretical fits to the data.

positions on the finite element grid and also low switching voltages are employed which do not cause large gradients in the n-director.

In Figure 6 the experimental x-dependence of the fringe displacement amplitude across the device is shown at two different times: 0.25 sec (circles) and 2.75 seconds (squares). The times correspond

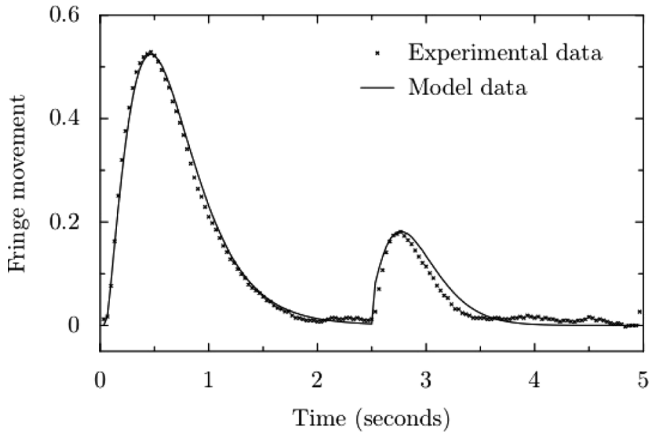

FIGURE 7 The crosses show experimental data for the relative fringe movement as a function of time at the position x = +17 μm, corresponding to a horizontal section through Figure 5. The solid line is theoretical fits to the data.

TABLE 1 Parameters Obtained from the Fit to the Interferometric Data for the Phase Grating Device with Parallel Surface Alignment (from the Current Work) and for the Device with Antiparallel Surface Alignment (from Reference [14])

	Parallel	Antiparallel [14]
Ion enhanced voltage, V_{pk}	1.89 V	1.89 V
Voltage decay time, τ	0.8 sec	0.8 sec
Surface pretilt, θ_p	0.4°	0.4°
Viscosity, γ_1	0.18 N s m^{-2}	0.18 N s m^{-2}
(e_1+e_3)	14 ± 1 pC m	15 ± 2 pC m

to 0.25 sec after a reversal of polarity of the applied squarewave voltage waveform to positive (circles) or negative (squares). This Figure effectively shows vertical cross sections through Figure 5 at the times given above. The crosses in Figure 7 shows the experimental time dependence of the fringe displacement amplitude at the position $x = +17\,\mu$m.

The solid lines in Figures 6 and 7 show theoretical fits to the interferometric data from Figure 5. Motivated by the transient capacitance results and the simulations in sections 2 and 3, the voltage experienced by the liquid crystal after the effect of ionic migration and shielding was taken into account was modelled by the function $V = V_{pk}\exp(-t/\tau)$ during each half period. The peak voltage will be enhanced above the applied voltage V_O by the reverse ionic field, as discussed in section 2, and the decay time τ is determined by the mobility of the ionic species and their effectiveness in shielding the applied voltage and the viscoelastic relaxation time of the nematic material. The elastic constant and permittivity values used to obtain the fits are the same as those listed in section 3. The other values that were used in the fitting for the parallel alignment geometry that has been studied here are shown in column 1 of Table 1.

6. DISCUSSION AND CONCLUSIONS

Table 1 compares the values obtained from fitting the interferometric data for the parallel geometry in the present work with the results from the antiparallel geometry that were reported in a previous publication [14]. The values used to obtain a fit for the two different cells were the same, and the values for the sum of the flexoelectric coefficients (e_1+e_3) are in agreement to within experimental errors. These results are also consistent with an analysis of results of Freedericksz measurements on the same material, E7, in reference

[30], and compare very well with the value $(e_1 + e_3) = 15 \pm 2$ pC m^{-1} found for the same material in reference [31].

One feature that is not accounted for in the modelling of the parallel geometry is the asymmetry between the peaks in the fringe displacement in Figure 6. The higher peak occurs at $x = -17\,\mu$m for a positive applied voltage (circles in Fig. 6), but the peak at $x = +17\,\mu$m (squares in Fig. 6) is higher for negative applied voltages. A single surface pretilt has been used in the theoretical model and it is possible that the pretilt on the two substrates are different due to the different underlying electrode structures on the two substrates. The use of an effective voltage in the 2 dimensional analysis of the phase grating data also neglects any effect from ion-director-polarisation coupling which would occur in the bulk of the device.

REFERENCES

[1] Chandrasekhar, S. (1992). *Liquid Crystals,* 2nd Edition, Cambridge University Press.
[2] de Gennes, P. G. & Prost, J. (1993) *The Physics of Liquid Crystals,* 2nd Edition, Clarendon Press: Oxford.
[3] Maier, W. & Saupe, A. (1960). *Z. Naturforsch, A*, *15*, 287.
[4] Meyer, R. B. (1969). *Phys. Rev. Lett.*, *22*, 918.
[5] Prost, J. & Pershan, P. S. (1976). *J. Appl. Phys.*, *47*, 2298.
[6] Madhusudana, N. V. & Durand, G. (1985). *J. Phys – Lettres*, *46*, L195.
[7] Valenti, B., Bertoni, C., Barbero, G., Taverna-Valabrega, P., & Bartolino, R. (1987). *Mol. Cryst. Liq. Cryst.*, *146*, 307.
[8] Blinov, L. M., Durand, G., & Yablonsky, S. V. (1992). *J. Phys. II France*, *2*, 1287.
[9] Warrier, S. R. & Madhusudana, N. V. (1997). *J. Phys. II France*, *7*, 1789.
[10] Mazzulla, A., Ciuchi, F., & Sambles, J. R. (2001). *Phys Rev E.*, *64*, 21708.
[11] Ponti, S., Ziherl, P., Ferrero, C., & Žumer, S. (1999). *Liquid Crystals*, *8*, 1171.
[12] Takahashi, T., Hashidate, S., Nishijou, N., Usui, M., Kimura, M., & Akahane, T. (1998). *Jap. Jour. Appl. Phys.*, *37*, 1865.
[13] Jewell, S. & Sambles, J. R. (2002). *J. Appl. Phys.*, *92*, 19.
[14] Trabi, C., Brown, C. V., Smith, A. A. T., & Mottram, N. J. (2008). *Appl. Phys. Lett.*, *92*, 223509.
[15] Hind, J. M., Smith, A. A. T., & Brown, C. V. (2006). *J. Appl. Phys.*, *100*(9), 094109.
[16] Horowitz, P. & Hill, W. (1987). *The Art of Electronics*, Cambridge University Press: Cambridge, p. 122.
[17] Freedericksz, V. & Zolina, V. (1933). *Trans. Faraday Soc.*, *29*, 919.
[18] Bradshaw, M. J. & Raynes, E. P. (1981). *Mol. Cryst. Liq. Cryst.*, *72*, 35.
[19] Mada, H. & Osajima, K. (1986). *J. Appl. Phys.*, *60*, 3111.
[20] Eriksen, J. L. (1961). *Trans. Soc. Rheol.*, *5*, 23.
[21] Leslie, F. M. (1992). *Continuum Mech. Thermodyn.*, *4*, 167.
[22] COMSOL Multiphysics, COMSOL Ltd, UH Innovation Centre, College Lane, Hatfield, Hertfordshire AL10 9AB, U.K.
[23] Smith, A. A. T., Brown, C. V., & Mottram, N. J. (2007). *Phys. Rev. E.*, *75*, 041704.
[24] Blinov, L. M., Kabayenkov, A. Y., & Sonin, A. A. (1989). *Liq. Cryst.*, *5*, 645.
[25] Barbero, G., Zvezdin, A. K., & Evangelista, L. R. (1999). *Phys. Rev. E.*, *59*, 1846.

[26] Born, M. & Wolf, E. (1980). *Principles of Optics*, Oxford: Pergamon.
[27] Kilian, A. & Hess, S. (1989). *Z. Naturforsch, 44a*, 693.
[28] Dickmann, S., Eschler, J., Cossalter, O., & Mlynski, D. A. (1993). *S.I.D. 1993 Technical Digest*, 638.
[29] Mori, H., Gartland, E. C., Kelly, J. R., & Bos, P. J. (1999). *Jpn. J. Appl. Phys.*, *38*, 135.
[30] Brown, C. V. & Mottram, N. J. (2003). *Phys. Rev. E.*, *68*(3), 31702.
[31] Jewell, S. & Sambles, J. R. (2002). *J. Appl. Phys.*, *92*, 19.